Int. J. Radiation Oncology Biol. Phys., Vol. 82, No. 5, pp. 1584–1593, 2012

0360-3016/$ - see front matter

ELSEVIER

doi:10.1016/j.ijrobp.2011.02.002

PHYSICS CONTRIBUTION

DEVELOPMENT AND CLINICAL EVALUATION OF A THREE-DIMENSIONAL CONE-BEAM COMPUTED TOMOGRAPHY ESTIMATION METHOD USING A DEFORMATION FIELD MAP

Lei Ren, Ph.D.,* Indrin J. Chetty, Ph.D.,* Junan Zhang, Ph.D.,‡ Jian-Yue Jin, Ph.D.,* Q. Jackie Wu, Ph.D.,† Hui Yan, Ph.D.,† David M. Brizel, M.D.,† W. Robert Lee, M.D.,† Benjamin Movsas, M.D.,* and Fang-Fang Yin, Ph.D.†

*Department of Radiation Oncology, Henry Ford Health System, Detroit, MI; †Department of Radiation Oncology, Duke University Medical Center, Durham, NC; and ‡Department of Radiation Oncology, Oregon Health and Science University, Portland, OR

Purpose: To develop a three-dimensional (3D) cone-beam computed tomography (CBCT) estimation method using a deformation field map, and to evaluate and optimize the efficiency and accuracy of the method for use in the clinical setting.

Methods and Materials: We propose a method to estimate patient CBCT images using prior information and a deformation model. Patients' previous CBCT data are used as the prior information, and the new CBCT volume to be estimated is considered as a deformation of the prior image volume. The deformation field map is solved by minimizing deformation energy and maintaining new projection data fidelity using a nonlinear conjugate gradient method. This method was implemented in 3D form using hardware acceleration and multi-resolution scheme, and it was evaluated for different scan angles, projection numbers, and scan directions using liver, lung, and prostate cancer patient data. The accuracy of the estimation was evaluated by comparing the organ volume difference and the similarity between estimated CBCT and the CBCT reconstructed from fully sampled projections.

Results: Results showed that scan direction and number of projections do not have significant effects on the CBCT estimation accuracy. The total scan angle is the dominant factor affecting the accuracy of the CBCT estimation algorithm. Larger scan angles yield better estimation accuracy than smaller scan angles. Lung cancer patient data showed that the estimation error of the 3D lung tumor volume was reduced from 13.3% to 4.3% when the scan angle was increased from 60° to 360° using 57 projections.

Conclusions: The proposed estimation method is applicable for 3D DTS, 3D CBCT, four-dimensional CBCT, and four-dimensional DTS image estimation. This method has the potential for significantly reducing the imaging dose and improving the image quality by removing the organ distortion artifacts and streak artifacts shown in images reconstructed by the conventional Feldkamp–Davis–Kress (FDK) algorithm. © 2012 Elsevier Inc.

Imaging dose reduction, Image reconstruction, Deformable registration, Image-guided radiation therapy, Cone-beam CT (CBCT).

INTRODUCTION

On-board cone-beam computed tomography (CBCT) is now becoming a powerful tool for image-guided radiation therapy (1), but its clinical utility may be limited because of its high imaging dose to a large volume of the patient (2). Specifically, in some adaptive radiation therapy contexts where CBCT is taken daily over a 30- to 40-fraction treatment, the accumulated imaging dose may have clinical significance.

Reducing the number of projections acquired in a CBCT scan is a rational strategy for reducing the imaging dose. Two different approaches have been taken to reduce the number of CBCT projections. The first approach, digital tomosynthesis (DTS), acquires projections only within a limited scan angle (20–60°) (3). Our previous studies showed that DTS images reconstructed by the Feldkamp–Davis–Kress (FDK) (4) method can provide accurate rigid body alignment of the patient's bony structures (5). However, DTS images do not provide full volumetric information for target localization due to the limited angle of the DTS acquisition. The second approach is to reduce the number of projections acquired without limiting the scan

Reprint requests to : Lei Ren, Ph.D., Department of Radiation Oncology, Henry Ford Health System, Detroit, MI 48202. Tel: (313) 916-1019; Fax: 313-916-3235; E-mail: lren1@hfhs.org

This paper was orally presented at the American Society for Radiation Oncology (ASTRO) 52nd Annual Meeting, San Diego, CA, October 31- November 4, 2010, as the recipient of the Basic Science Abstract Award.

Supplementary material for this article can be found at www.redjournal.org.

Conflict of interest: none.

Received May 7, 2009, and in revised form Jan 28, 2011. Accepted for publication Feb 2, 2011.

angle. The CBCT images reconstructed by the FDK method in this approach usually have severe streak artifacts because of the limited amount of projection information acquired.

Novel image reconstruction methods have been developed recently to improve the image quality for reconstruction using undersampled projection data. One category of methods is based on the compressed sensing (CS) theory (6), and it has been implemented for image reconstruction from limited-views and limited-angle projection data (7–9). However, these methods generally assume the images studied to be sparse which may not always be true for medical images. Besides, these methods can not recover the full volumetric information in DTS images or completely remove the streak artifacts in limited projection CBCT reconstruction when the projection number is small. Furthermore, the image resolution is often degraded in these methods. Another category of methods uses deformable image registration for image reconstruction (10–16) These methods were mainly developed for four-dimensional (4D) CT and 4D CBCT image reconstruction, and no such method has been comprehensively evaluated for limited-angle DTS reconstruction. Previously we developed a novel CBCT estimation method that uses a deformation field map to estimate CBCT images from limited-angle projections (17). However, this method was developed and tested only in two-dimensional (2D) cases, and it was not clear whether it is feasible for estimation of 3D CBCT images using limited projections.

In the current study, we implemented the method in 3D form using hardware acceleration and multi-resolution scheme, and evaluated it both for limited-angle and for limited-projection image reconstruction using liver, lung, and prostate cancer patient data. Comprehensive evaluation of the effects of projection number, scan angle, and scan direction on the CBCT estimation accuracy was performed, and different estimation parameters of the proposed method were optimized for clinical use.

METHODS AND MATERIALS

CBCT estimation algorithm

Either patient planning CT images or the previous day's CBCT images can be used as the prior images, which are denoted by I_{prior}. The new 3D CBCT images to be estimated are denoted by $CBCT_{new}$. The size of these images is defined to be n×n×n. In our method, the $CBCT_{new}$ image is considered as a deformation of the prior image I_{prior}. The deformation field is represented by $D_m(k,j,i)$, $m = 1,2,3$, $k,j,i = 1...\ n$, where m represent the three directional components of the deformation field along x, y, and z axes, respectively, and k, j, and i represent the 3D index of the deformation field at each image voxel. Then $CBCT_{new}$ can be expressed as a function of D and I_{prior} as follows:

$$CBCT_{new} = CBCT_{new}\left(D,\ I_{prior}\right) \tag{1}$$

Specifically, each voxel value in $CBCT_{new}$ is interpolated from I_{prior} according to the deformation field D using trilinear interpolation. The equation for calculating the voxel value at (k, j, i) in the new CBCT image is as follows:

$$CBCT_{new}\ (k,j,i) = I_{prior}\ (k + D_1(k,j,i),\ j + D_2(k,j,i),\ i + D_3(k,j,i)) \tag{2}$$

In image reconstruction, the data fidelity constraint has to be met, which can be expressed by the following equation:

$$P^{*}\ CBCT_{new}\ \left(D,\ I_{prior}\right) = Y \tag{3}$$

where P is the cone-beam projection matrix to describe the x-ray projection measurements, and Y is the new cone-beam projection data acquired. Another constraint that we used to solve the deformation field is the energy constraint, which requires the deformation field D to have the minimum deformation energy. We used the free-form energy defined by Lu *et al.* (18) as the deformation energy. The formula of the free-form energy is as follows:

$$E(D) = \sum_{k=1}^{n}\sum_{j=1}^{n}\sum_{i=1}^{n}\sum_{m=1}^{3}\left(\left(\frac{\partial D_m(k,j,i)}{\partial x}\right)^2 + \left(\frac{\partial D_m(k,j,i)}{\partial y}\right)^2 + \left(\frac{\partial D_m(k,j,i)}{\partial z}\right)^2\right) \tag{4}$$

Based on these two constraints, the CBCT estimation problem is converted into the following unconstrained optimization problem:

$$\tilde{D} = \arg\min_{\forall D} f(D) = \arg\min_{\forall D}\left(\mu * E(D) + \left\|P * CBCT_{new}\left(D, I_{prior}\right) - Y\right\|_2^2\right) \tag{5}$$

where f(D) is the objective function to be minimized, and μ is the relative weight of the deformation energy. A nonlinear conjugate gradient (CG) method is used as the optimizer to solve the optimization problem in Eq. (5) (19). After the deformation field D is solved, the new on-board CBCT image $CBCT_{new}$ is obtained by deforming the prior image I_{prior} based on Eq. (2).

Hardware acceleration

This 3D CBCT estimation algorithm requires forward projection and back projection of the 3D volume in each iteration loop. The forward projection process that generates digital reconstructed radiographs (DRR) is the most time-consuming process. We have implemented this process in the computer graphics card to accelerate its speed (20). By using the three color channels in the graphics card, we are able to extend its data storage range to 0 to 2047 (11-bit). For CBCT estimation using simulated projections of the new CBCT images, both I_{prior} and the new CBCT images are linearly scaled to a data range of 0 to 2,047 before generating DRRs from deformed I_{prior} and simulated new projections from new CBCT images. For CBCT estimation using real cone-beam projections, the DRRs need to be generated from deformed I_{prior} with its original gray value range to match the gray value range of real projection images to meet the data fidelity constraint. To achieve that, we first linearly scale the gray values of the I_{prior} into 11-bit range by using the following formula:

$$I_{prior}{}' = \left(I_{prior} - I_{prior}{}^{min}\right) \Big/ \left(I_{prior}{}^{max} - I_{prior}{}^{min}\right) * 2047 \tag{6}$$

The scaled image volume I'_{prior} is loaded into the three color channels in the computer graphics card. The image volume is

then resliced into 256 slices and projected onto the detector plane slice by slice based on the cone-beam geometry. The DRR' of I'_{prior} is the summation of these projections. Because this DRR generation process is a linear process, the DRR' of I'_{prior} and the DRR of the original I_{prior} share the same relationship as that between I'_{prior} and I_{prior} in Eq. (6). Therefore, the DRR of I_{prior} can be calculated according to the following equation:

$$DRR = DRR'/2047 * \left(I_{prior}^{max} - I_{prior}^{min}\right) + I_{prior}^{min} \quad (7)$$

Multi-resolution scheme

A multi-resolution scheme is used to improve the speed, robustness, and accuracy of the estimation algorithm. As shown in Fig. 1, the $CBCT_{prior}$ image is downsampled into different resolution levels. The CBCT estimation is performed first at the coarsest resolution level, and the starting point of the deformation field is set to be zero. After convergence, the algorithm proceeds to higher resolution levels, and finally at full resolution level. At each higher resolution level, the starting point of the deformation field is obtained by expanding the deformation field solved from the previous lower resolution level. Linear interpolation is used to expand the deformation field. In our study, three levels of resolution are used in the scheme, and the $CBCT_{prior}$ image volume is downsampled by a factor of 2 along each dimension for each lower resolution level.

Evaluation methods

The new CBCT images reconstructed from fully sampled projection images are considered as the ground truth for evaluating the estimation accuracy, and they are denoted as $CBCT_{new}^{0}$. The estimation accuracy was quantitatively evaluated by calculating the organ volume percentage difference and the similarity between the estimated $CBCT_{new}$ images and the $CBCT_{new}^{0}$ images.

The organ volume percentage difference is calculated as follows:

$$\text{Organ volume percentage difference} = \frac{|(V \cup V_0 - V \cap V_0)|}{|V_0|} \quad (8)$$

where V is the 3D organ volume contoured in the estimated $CBCT_{new}$ images, and V_0 is the 3D organ volume contoured in the $CBCT_{new}^{0}$ images.

The similarity between the estimated $CBCT_{new}$ images and the $CBCT_{new}^{0}$ images was evaluated by the cross-correlation (CC) and mutual information (MI) between the two sets of images. Cross-correlation is calculated as follows:

$$CC(X,Y) = \frac{\sum_{k=1}^{n}\sum_{j=1}^{n}\sum_{i=1}^{n}(X(k,j,i) - mean(X)) * (Y(k,j,i) - mean(Y))}{\sqrt{\left(\sum_{k=1}^{n}\sum_{j=1}^{n}\sum_{i=1}^{n}(X(k,j,i) - mean(X))^2\right) * \left(\sum_{k=1}^{n}\sum_{j=1}^{n}\sum_{i=1}^{n}(Y(k,j,i) - mean(Y))^2\right)}} \quad (9)$$

where X and Y are the estimated $CBCT_{new}$ and the $CBCT_{new}^{0}$ images respectively. Mutual information is calculated as follows:

$$MI(X,Y) = \sum_{y \in Y}\sum_{x \in X} p(x,y)\log_2\frac{p(x,y)}{p(x) * p(y)} \quad (10)$$

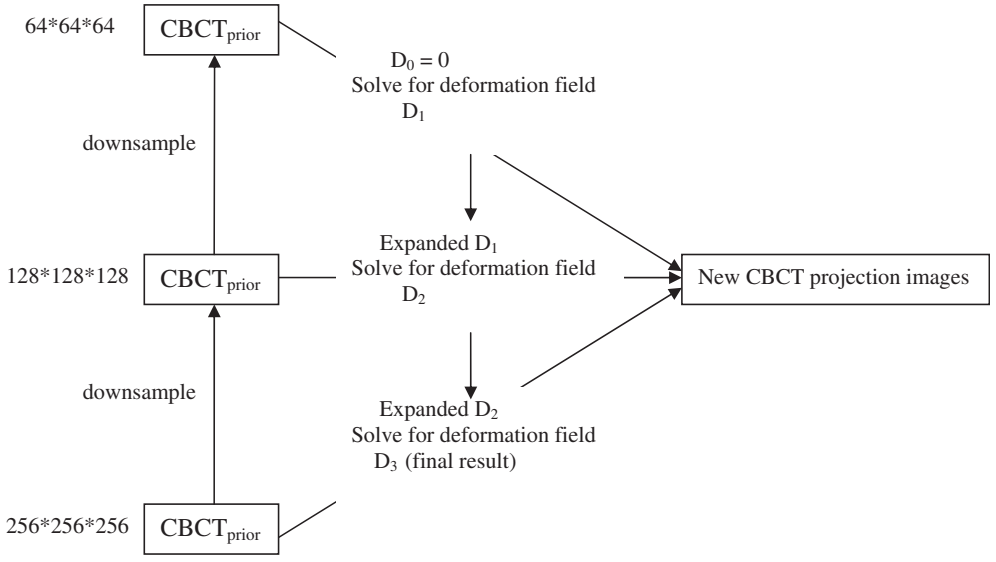

Fig. 1. Multi-resolution scheme used in the cone-beam computed tomography (CBCT) estimation algorithm: the $CBCT_{prior}$ image is downsampled into different levels, the estimation proceeds from the coarsest resolution level to the full resolution level, at each level the starting point of the deformation field is obtained by expanding the deformation field solved from the previous lower resolution level.

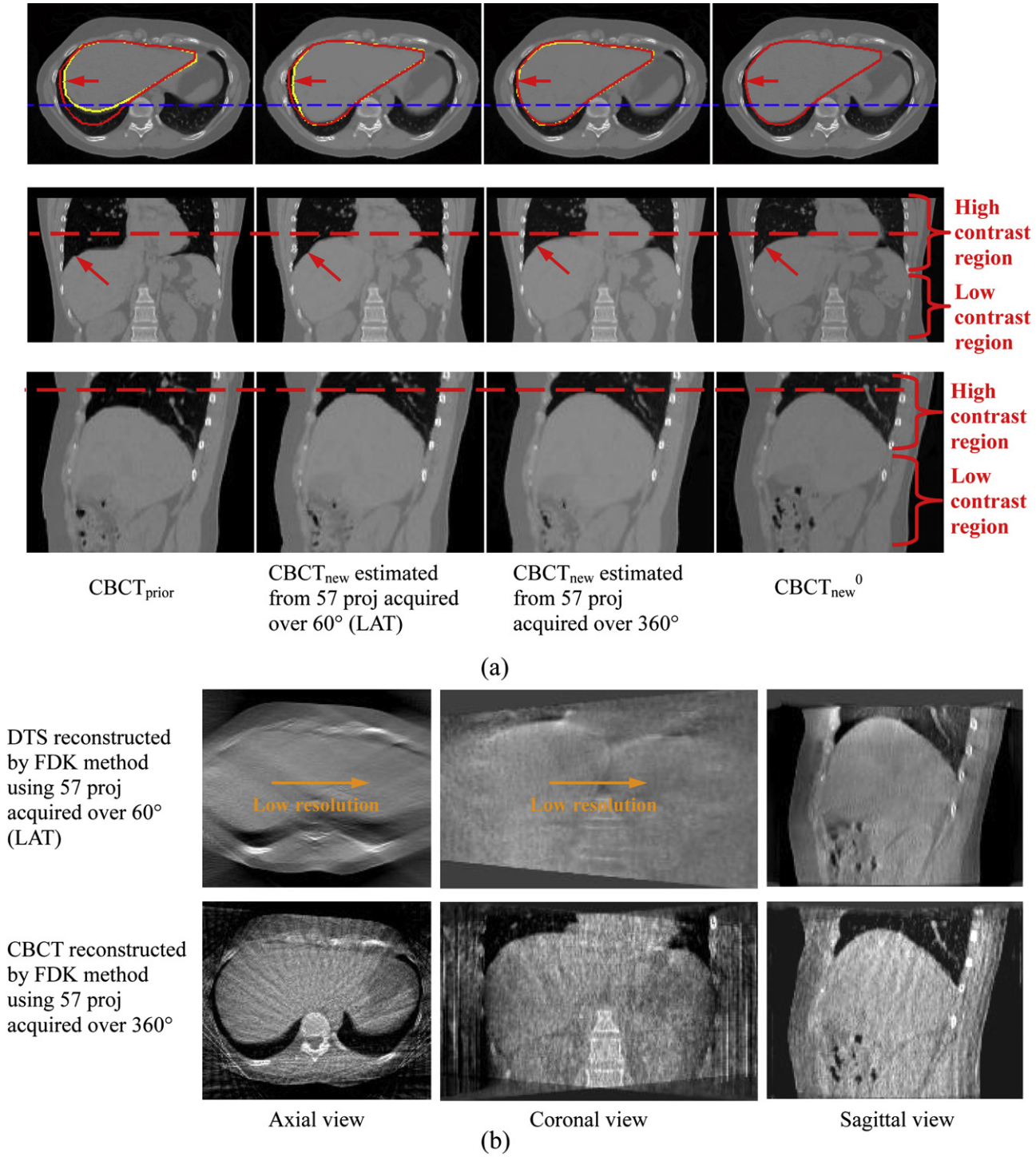

Fig. 2. Prior image–based and Feldkamp–Davis–Kress (FDK) method–based CBCT$_{new}$ images of liver cancer patient data. In the axial view images in (a), the contour of liver in CBCT$_{new}^{0}$ (red contour) is overlaid onto CBCT$_{prior}$ and estimated CBCT$_{new}$ images for comparison with the liver contours in these images (yellow contours). In coronal and sagittal view images in (a), the dashed red lines indicate the height of the diaphragm in CBCT$_{new}^{0}$. The low-contrast region is mainly in the abdominal region, as indicated in (a). CBCT = cone-beam computed tomography.

where X and Y are the estimated CBCT$_{new}$ and the CBCT$_{new}^{0}$ images respectively, p(x) and p(y) are the normalized histograms of X and Y separately, and p(x, y) is the normalized joint histogram of X and Y.

This 3D CBCT estimation method was tested both for limited-angle and for limited-projection image reconstruction using liver, lung, and prostate patient data. Comprehensive evaluations of the effects of the number of projections, scan angle, and scan direction on the CBCT estimation accuracy were performed, and different estimation parameters of the proposed method were optimized for clinical use.

Table 1. Three-dimensional (3D) liver and lung volume percentage difference, diaphragm height difference, cross-correlation (CC), and mutual information (MI) between $CBCT_{new}^{0}$ and $CBCT_{new}$ images estimated from different number of projections acquired over different scan angles along different directions in a liver cancer patient study

	3D liver volume % difference						
	Total % difference	High–contrast region	Low–contrast region	3D lung volume % difference	Diaphragm height difference (mm)	CC	MI
$CBCT_{prior}$	33.9%	18.2%	15.7%	25.9%	18.4	0.83	1.38
Total scan angle of 30°							
15 proj over 30° (LAT)	22.5%	9.5%	13.0%	16.1%	6.8	0.89	1.43
30 proj over 30° (LAT)	22.4%	9.4%	13.0%	16.3%	6.8	0.89	1.43
57 proj over 30° (LAT)	21.7%	8.8%	12.9%	16.6%	6.8	0.88	1.41
57 proj over 30° (AP)	22.0%	9.0%	13.0%	16.9%	6.8	0.89	1.42
57 proj over 30° (Oblique)	22.1%	9.2%	12.9%	17.1%	6.8	0.88	1.42
15 proj over dual 15°	21.0%	7.9%	13.1%	14.0%	5.1	0.92	1.45
57 proj over dual 15°	19.2%	6.4%	12.8%	10.9%	5.1	0.94	1.54
Total scan angle of 60°							
30 proj over 60° (LAT)	19.6%	6.5%	13.1%	12.6%	5.1	0.92	1.53
57 proj over 60° (LAT)	18.7%	5.9%	12.8%	11.4%	3.4	0.93	1.58
112 proj over 60° (LAT)	19.5%	6.7%	12.8%	12.7%	5.1	0.92	1.52
112 proj over 60° (AP)	18.9%	6.2%	12.7%	11.9%	5.1	0.93	1.53
112 proj over 60° (Oblique)	19.5%	6.6%	12.9%	12.4%	5.1	0.92	1.52
30 proj over dual 30°	20.5%	7.5%	13.0%	11.8%	5.1	0.94	1.52
112 proj over dual 30°	19.4%	6.6%	12.8%	10.9%	5.1	0.95	1.58
Total Scan Angle of 90°							
45 proj over 90° (LAT)	18.5%	5.6%	12.9%	9.0%	3.4	0.95	1.64
90 proj over 90° (LAT)	18.9%	6.2%	12.7%	11.0%	3.4	0.94	1.57
166 proj over 90° (LAT)	18.8%	6.1%	12.7%	11.1%	5.1	0.93	1.58
166 proj over 90° (AP)	19.3%	6.4%	12.9%	11.5%	3.4	0.91	1.57
166 proj over 90° (Oblique)	19.5%	6.6%	12.9%	11.7%	5.1	0.92	1.58
45 proj over dual 45°	17.7%	5.1%	12.6%	7.6%	3.4	0.97	1.66
166 proj over dual 45°	17.1%	4.7%	12.4%	7.4%	3.4	0.96	1.66
Total scan angle of 360°							
57 proj over 360°	13.7%	1.6%	12.1%	5.2%	1.7	0.98	1.78
112 proj over 360°	13.5%	1.7%	11.8%	5.2%	1.7	0.98	1.79
166 proj over 360°	13.5%	1.8%	11.7%	6.2%	1.7	0.97	1.72

Abbreviations: AP = anterior–posterior; CBCT = cone-beam computed tomography; LAT = lateral; proj = projections.
Voxel size for CBCT images is 1.7 × 1.7 × 1.7 mm.

RESULTS

CBCT estimation of liver cancer patient data

The 4D CT images of a liver cancer patient at inhale and exhale phases were used as $CBCT_{prior}$ and $CBCT_{new}^{0}$ images to simulate an extreme case of soft tissue deformation. Projections simulated from $CBCT_{new}^{0}$ were used for CBCT estimation. Figure 2a shows the axial, coronal, and sagittal views of the $CBCT_{prior}$, $CBCT_{new}^{0}$, and estimated $CBCT_{new}$ images. In the axial view images, the liver contour in the $CBCT_{new}^{0}$ images (red contour) is overlaid onto the $CBCT_{prior}$ and estimated $CBCT_{new}$ images for comparison with the liver contours in these images (yellow contours). In coronal and sagittal view images, the dashed red lines indicate the height of the diaphragm in $CBCT_{new}^{0}$. The DTS and CBCT images reconstructed by the FDK method using limited projections are shown in Fig. 2(b). Severe organ distortion and streak artifacts were observed in the FDK-based DTS and CBCT images, respectively. Fig. E1 shows a comparison of line profiles in $CBCT_{prior}$, $CBCT_{new}^{0}$, and estimated $CBCT_{new}$ images. The location of the line profile is indicated by the blue dashed lines in the axial view images in Fig. 2a.

To quantitatively evaluate the accuracy of the estimation algorithm, the 3D liver volume was manually contoured, and the liver volume percentage difference between estimated $CBCT_{new}$ and $CBCT_{new}^{0}$ was calculated using Eq. (**8**). To investigate the performance of this algorithm in estimating organ volumes in regions of different contrast, we divided the liver patient volume into a high-contrast region and low-contrast region, as shown in the coronal and sagittal views of Fig. 2a. The high-contrast region is in the upper part of body where there is high contrast between liver and adjacent lung volume, and the low-contrast region is in the lower abdominal region where there is low contrast between liver and adjacent abdominal organs that have intensity values similar to those of the liver.

The summation of liver volume percentage difference in the low- and high-contrast regions is equal to the total liver volume percentage difference. Although the whole lung was not imaged, the partial lung volumes were also contoured using automatic thresholding followed by manual adjustment, and lung volume percentage difference between estimated $CBCT_{new}$ and $CBCT_{new}^{0}$ was calculated. Table 1 shows

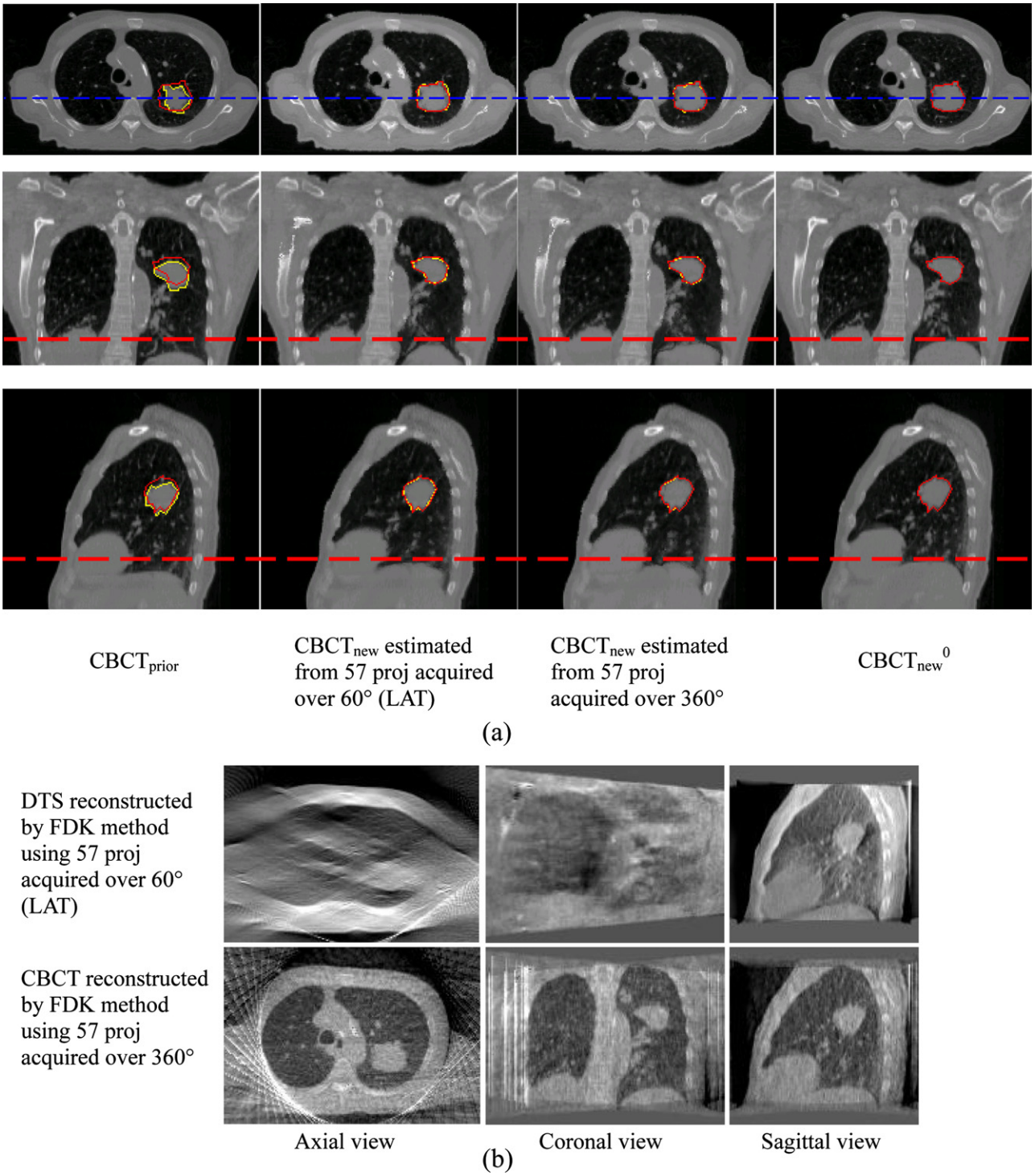

Fig. 3. Prior image–based and Feldkamp–Davis–Kress (FDK) method–based CBCT$_{new}$ images of lung cancer patient data. In the axial, coronal, and sagittal view images in (a), the contours of the lung tumor in CBCT$_{new}^{0}$ (red contours) are overlaid onto CBCT$_{prior}$ and estimated CBCT$_{new}$ images for comparison with the lung tumor contours in these images (yellow contours). In coronal and sagittal view images in (a), the dashed red lines indicate the height of the diaphragm in CBCT$_{new}^{0}$. CBCT = cone-beam computed tomography.

the results for liver and lung volume percentage difference, diaphragm height difference, CC, and MI between estimated CBCT$_{new}$ and CBCT$_{new}^{0}$ images. The results for CBCT$_{prior}$ are the volume difference and similarity between CBCT$_{prior}$ and CBCT$_{new}^{0}$ images. Different scan angles, scan directions, and number of projections were tested to evaluate their effects on the estimation accuracy. As shown in Fig. E2, the scan directions tested include anterior–posterior (AP), lateral (LAT), Oblique (45° tilt), and Dual angle (AP+LAT). The dual-angle scan was used to simulate the image

Table 2. Three-dimensional (3D) lung tumor volume percentage difference between $CBCT_{prior}$, estimated $CBCT_{new}$ and $CBCT_{new}^{0}$ in 8 lung cancer patients' data

Patient no.	$CBCT_{prior}$	$CBCT_{new}$ estimated from 57 projections over 60° (LAT)	$CBCT_{new}$ estimated from 57 projections over 360°	Tumor volume in $CBCT_{new}^{0}$ (cc)
1	54.2%	14.1%	3.4%	36.1
2	57.0%	19.2%	3.6%	15.2
3	77.4%	5.9%	4.2%	4.1
4	18.0%	4.5%	2.1%	39.0
5	48.4%	4.8%	2.6%	51.9
6	26.7%	13.0%	4.2%	36.1
7	178.9%	30.5%	8.3%	6.1
8	79.2%	14.1%	5.6%	3.7
Mean	67.5%	13.3%	4.3%	24.0
SD	49.9%	8.8%	2.0%	18.9

Abbreviations: LAT = lateral; SD = standard deviation.
Voxel size for CBCT images is approximately 2 × 2 ×2 mm.

acquisition in the dual-source CBCT imaging system, and its total scan angle was set to be the same as single-angle scans. From Table 1, we noted the following: (*1*) The algorithm has better estimation accuracy in the high-contrast region than in the low-contrast region. (*2*) The total scan angle is the dominant factor affecting the estimation accuracy. Increasing the scan angle improves the estimation accuracy. (*3*) The number of projections and scan direction do not have significant effects on the estimation accuracy.

CBCT estimation of lung cancer patient data

The 4D CT images of lung cancer patients at inhale and exhale phases were used as $CBCT_{prior}$ and $CBCT_{new}^{0}$ images to simulate extreme cases of soft tissue deformation. Projections simulated from $CBCT_{new}^{0}$ were used for CBCT estimation. Eight lung cancer patients' data were tested, and 57 projections acquired over 60° and 360° were used for CBCT estimation in each patient. Figure 3a shows one example of the axial, coronal, and sagittal views of the $CBCT_{prior}$, $CBCT_{new}^{0}$, and estimated $CBCT_{new}$ images. In all three views, the lung tumor contours in the $CBCT_{new}^{0}$ images (red contour) are overlaid onto the $CBCT_{prior}$ and estimated $CBCT_{new}$ images for comparison with the lung tumor contours in these images (yellow contours). In coronal and sagittal view images, the red dashed lines indicate the height of the diaphragm in $CBCT_{new}^{0}$. The DTS and CBCT images reconstructed by the FDK method are shown in Fig. 3b. Figure E3 shows a comparison of line profiles in $CBCT_{prior}$, $CBCT_{new}^{0}$, and estimated $CBCT_{new}$ images. The location of the line profile is indicated by the blue dashed lines in the axial view images in Fig. 3a.

For quantitative evaluation of the estimation accuracy, the 3D lung tumor volume was manually contoured and the tumor volume percentage difference between $CBCT_{prior}$, estimated $CBCT_{new}$ and $CBCT_{new}^{0}$ was calculated. The CC and MI were also calculated to evaluate the pixel value similarity between estimated $CBCT_{new}$ and $CBCT_{new}^{0}$ images. The results for tumor volume percentage difference are shown in Table 2, and the results for CC and MI are shown in Table E1.

CBCT estimation of prostate cancer patient data

In the prostate cancer patient study, CBCT images acquired on different days for 8 prostate cancer patients were used as the $CBCT_{prior}$ and $CBCT_{new}^{0}$ images. Real cone-beam projection images were used for CBCT estimation. Eight prostate cancer patients' data were tested, and 57 projections acquired over 60° and 360° were used for CBCT estimation in each patient. Figure 4a shows an example of the axial, coronal, and sagittal views of the $CBCT_{prior}$, $CBCT_{new}^{0}$, and estimated $CBCT_{new}$ images. Red arrows in Fig. 4a indicate the gas filling change in the rectum from $CBCT_{prior}$ to $CBCT_{new}^{0}$ and the estimation of this change in the estimated $CBCT_{new}$ images. The DTS and CBCT images reconstructed by the FDK method are shown in Fig. 4b. The results for rectal volume percentage difference are shown in Table 3. The results for CC and MI are shown in Table E2.

DISCUSSION

Effects of scan angle, scan direction, and number of projections on the estimation accuracy

Results for the liver cancer patient study in Table 1 showed that, for a fixed scan angle (30°, 60°, 90°, or 360°), the scan direction (AP, LAT, or Oblique) and the number of projections do not have significant effects on the CBCT estimation accuracy. The dual-angle scans yield slightly better estimation accuracy than single-angle scans for the same total scan angle. The total scan angle is the dominant factor affecting the accuracy of the CBCT estimation algorithm. The estimation accuracy is improved as the total scan angle increases. It is also noted in Table 1 that the estimation accuracy of the liver volume in the low-contrast region did not improve much as scan angles increased from 30° to 360°, which shows that the current algorithm is less sensitive in detecting the organ deformations in the low-contrast regions. The data regarding 8 lung cancer patients and 8 prostate cancer patients also showed improvements on estimation accuracy for lung tumor volume and rectal volume when the scan angle was increased from 60° to 360° using 57 projections.

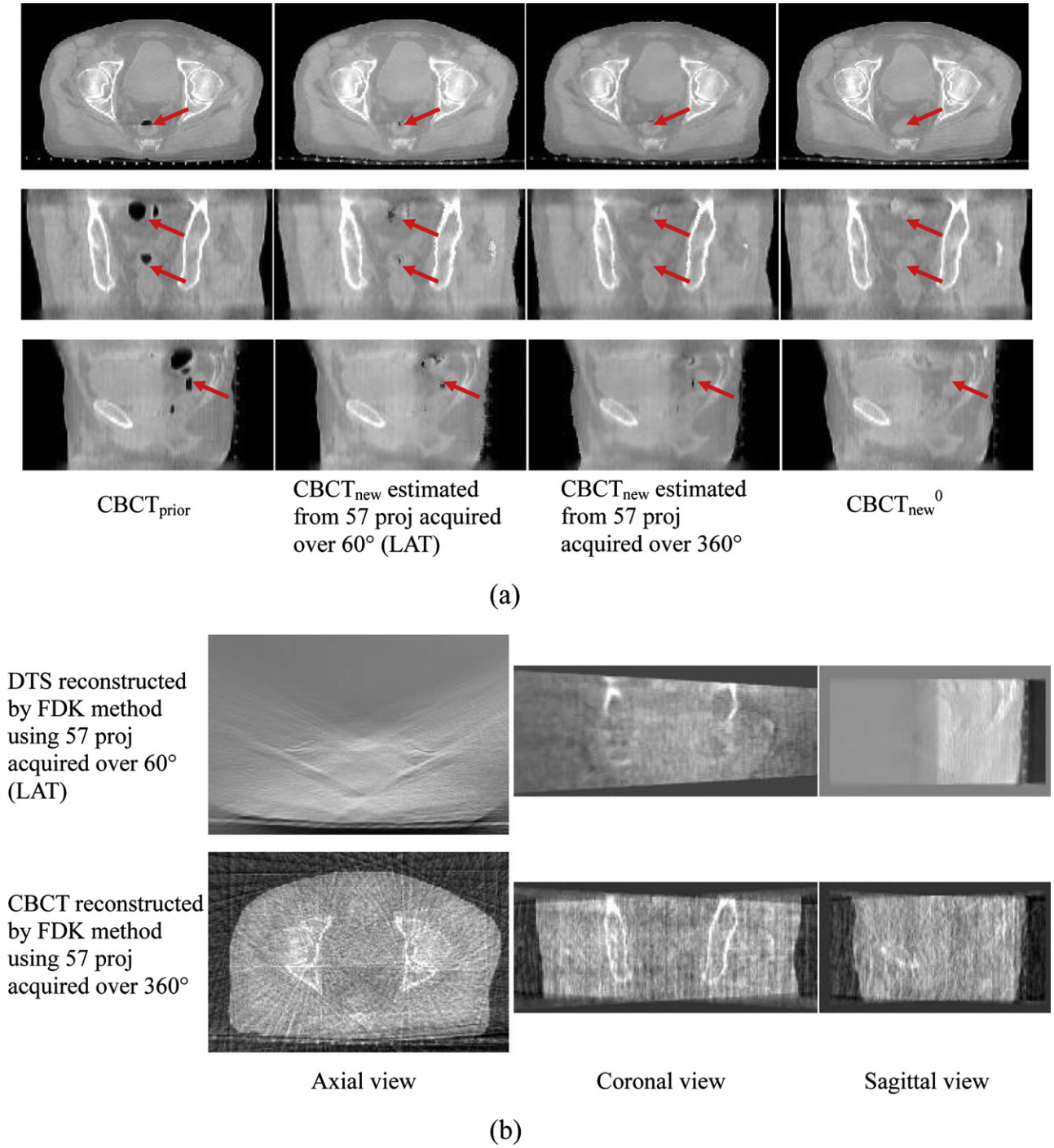

Fig. 4. Prior image–based and Feldkamp–Davis–Kress (FDK) method–based CBCT$_{new}$ images of prostate cancer patient data. Arrows in the figure (a) indicate the gas filling change in the rectum from CBCT$_{prior}$ to CBCT$_{new}^{0}$ and the estimation of this change in the estimated CBCT$_{new}$ images (b). CBCT = cone-beam computed tomography.

The reason for reduced estimation accuracy using a limited scan angle is that the projections acquired within the limited scan angle have limited information about the variation of patient anatomy along the depth direction, which is the direction along the central line of the scan angle. As shown in Fig. 2, in the estimated CBCT$_{new}$ images using lateral 60° scan angle, the depth direction is the patient lateral direction and the projections acquired have limited information about the anatomical variation along this lateral direction. As an extreme case, if only one projection is taken laterally, then all the anatomical structures at different lateral positions are projected onto one projection (virtually the lateral port film) and there is no information about the lateral position of each structure in this projection image. Because of this lack of depth information, the liver volume change along the lateral direction in the CBCT$_{new}$ image (as indicated by the red arrow in Fig. 2a) was not fully estimated using lateral 60° projections. For the same reason, the DTS

Table 3. Three-dimensional (3D) rectum volume percentage difference between $CBCT_{prior}$, estimated $CBCT_{new}$ and $CBCT_{new}{}^{0}$ in 8 prostate cancer patients' data

Patient no.	$CBCT_{prior}$	$CBCT_{new}$ estimated from 57 projections over 60° (LAT)	$CBCT_{new}$ estimated from 57 projections over 360°
1	103.0%	19.6%	5.8%
2	69.3%	14.5%	5.2%
3	75.8%	28.7%	4.9%
4	93.2%	22.8%	1.9%
5	80.2%	15.6%	5.3%
6	62.6%	9.1%	4.2%
7	41.5%	5.9%	3.0%
8	120.1%	25.1%	4.4%
Average	80.7%	17.7%	4.3%
SD	24.6%	7.9%	1.3%

Abbreviations: CBCT = cone-beam computed tomography; SD = standard deviation.

Voxel size for CBCT images is approximately 2 × 2 ×2 mm.

images reconstructed by the FDK method using lateral 60° projections showed much poorer resolution along the lateral direction than the AP and superior–inferior (SI) directions.

It should be noted that the conclusion that the number of projections does not have significant effects on the estimation accuracy is made only for the different numbers of projections tested in this study. It is evident that as the number of projections keeps decreasing, ultimately there will be not enough information acquired in the projections to estimate the new CBCT volume. The estimation accuracy will be impaired after the projection number is reduced below a certain level. The minimum number of projections required to maintain the estimation accuracy is dependent on the complexity of the structures to be estimated and the amount of deformation from $CBCT_{prior}$ to $CBCT_{new}$. Based on the results in liver, lung, and prostate cancer patient study, 57 projections acquired over 360° are sufficient to estimate the CBCT volume accurately.

Limitation and future developments of the CBCT estimation method

The results in the liver cancer patient study showed that the current algorithm is relatively less sensitive in detecting the organ deformations in the low-contrast regions. We can potentially improve the estimation accuracy in the low-contrast region by improving the optimization algorithm and the deformation model. The current deformation model is the intensity-based free-form energy, which has 3*N degrees of freedom (N is the number of voxels in the CBCT volume). This large number of variables dramatically increases the complexity of the optimization and makes the optimization algorithm less efficient in minimizing the objective function value, especially in the low-contrast region, where the gradient of the objective function is small. To solve this problem, other deformation models will be tested in future studies to reduce the degrees of freedom in the optimization, such as contour-based and control point–based deformation models. These feature-based models can be used alone or in combination with the intensity-based models to reduce the number of variables, which can potentially help the optimization to achieve better estimation accuracy with even fewer projections.

Potential applications of the CBCT estimation method

In DTS imaging, the proposed method is able to generate images without organ distortion artifacts shown in conventional DTS images and to provide reasonable estimation of the on-board patient volume using limited-angle projections.

In 3D CBCT imaging, this method is able to dramatically reduce the number of projections required without introducing streak artifacts shown in the conventional CBCT images reconstructed by the FDK method using limited projections. Results showed that 57 projections acquired over 360° scan angle are sufficient to provide accurate estimation of the CBCT volume using the proposed method, which are only one-tenth of the projections acquired in a conventional CBCT scan. This implies a 10-fold reduction of the imaging dose to the patient, making it more feasible to perform daily image guidance for patient treatment.

In 4D CBCT imaging, there are usually a very limited number of projections acquired for each phase, which lead to severe streak artifacts in the CBCT images reconstructed for each phase using the FDK method. The proposed method is able to provide accurate estimation of the CBCT images in each phase without introducing streak artifacts using even less imaging dose than a conventional 3D CBCT scan. This is especially useful for imaging lung cancer patients. Based on the lung tumor volume estimated by the proposed method for each phase, the on-board Internal Target Volume ITV volume of the lung tumor can be accurately generated and used for target localization. The improvement of localization accuracy can potentially allow us to further reduce the ITV to planning target volume margin used in the treatment planning process. The high-quality 4D CBCT images generated can also be used for 4D dose calculation and accumulation to track the actual dose delivered to the lung tumor for adaptive radiation therapy.

Potentially, this method can also be used for 4D DTS image estimation, where 4D projections are acquired within a limited scan angle. In addition, the deformation field solved during the estimation can be used as deformable registration results for tumor localization and dose tracking.

CONCLUSION

A 3D CBCT estimation method using a deformation field map was developed. Hardware acceleration and multiresolution scheme were used to improve the efficiency and accuracy of the algorithm. The method was evaluated using liver, lung, and prostate cancer patient data. The effects of number of projections, scan angle, and scan direction on the CBCT estimation accuracy were studied. Results showed that the scan direction (AP, LAT, or Oblique) and the number of projections do not have significant effects on the CBCT

estimation accuracy. The total scan angle is the dominant factor affecting the accuracy of the CBCT estimation algorithm. Larger scan angles yield better estimation accuracy than smaller scan angles. Lung cancer patient data showed that 57 projections acquired over a 360° scan angle are sufficient to provide accurate estimation of the tumor volume using the proposed method. This method is applicable for 3D DTS, 3D CBCT, 4D CBCT, and 4D DTS image estimation. The method has the potential for significantly reducing the imaging dose and improving the image quality by removing the organ distortion artifacts and streak artifacts shown in conventional images reconstructed by the FDK method.

REFERENCES

1. Dawson LA, Jaffray DA. Advances in image-guided radiation therapy. *J Clin Oncol* 2007;25:938–946.
2. Islam MK, Purdie TG, Norrlinger BD, *et al*. Patient dose from kilovoltage cone beam computed tomography imaging in radiation therapy. *Med Phys* 2006;33:1573–1582.
3. Godfrey DJ, Yin FF, Oldham M, *et al*. Digital tomosynthesis with an on-board kilovoltage imaging device. *Int J Radiat Oncol Biol Phys* 2006;65:8–15.
4. Feldkamp LA, Davis LC, Kress JW. Practical cone-beam algorithm. *J Opt Soc Am A* 1984;1:612–619.
5. Ren L, Godfrey DJ, Yan H, *et al*. Automatic registration between reference and on-board digital tomosynthesis images for positioning verification. *Med Phys* 2008;35:664–672.
6. Lustig M, Donoho D, Pauly JM. Sparse MRI: The application of compressed sensing for rapid MR imaging. *Magn Reson Med* 2007;58:1182–1195.
7. Choi K, Wang J, Zhu L, *et al*. Compressed sensing based cone-beam computed tomography reconstruction with a first-order method. *Med Phys* 2010;37:5113–5125.
8. Chen GH, Tang J, Leng S. Prior image constrained compressed sensing (PICCS): A method to accurately reconstruct dynamic CT images from highly undersampled projection data sets. *Med Phys* 2008;35:660–663.
9. Sidky EY, Kao CM, Pan X. Accurate image reconstruction from few-views and limited-angle data in divergent-beam CT. *J. X-Ray Sci Technol* 2006;14:119–139.
10. Li T, Koong A, Xing L. Enhanced 4D cone-beam CT with inter-phase motion model. *Med Phys* 2007;34:3688–3695.
11. Zeng R, Fessler JA, Balter JM. Respiratory motion estimation from slowly rotating x-ray projections: theory and simulation. *Med Phys* 2005;32:984–991.
12. Zeng R, Fessler JA, Balter JM. Estimating 3D respiratory motion from orbiting views by tomographic image registration. *IEEE Trans Med Imaging* 2007;26:153–163.
13. Badea CT, Schreibmann E, Fox T. A registration based approach for 4D cardiac micro-CT using combined prospective and retrospective gating. *Med Phys* 2008;35:1170–1179.
14. Docef A, Murphy M, Keall P, *et al*. Forward CT reconstruction from limited projection data. In: Proceedings of the 19th Conference on Computer-Assisted Radiology and Surgery, 2005, pp 104-108.
15. Brock RS, Docef A, Murphy MJ. Reconstruction of a cone-beam CT image via forward iterative projection matching. *Med Phys* 2010;37:6212–6220.
16. Long Y, Fessler JA, Balter JM. Accuracy estimation for projection-to-volume targeting during rotational therapy: a feasibility study. *Med Phys* 2010;37:2480–2490.
17. Ren L, Zhang J, Thongphiew D, *et al*. A novel digital tomosynthesis (DTS) reconstruction method using a deformation field map. *Med Phys* 2008;35:3110–3115.
18. Lu W, Chen ML, Olivera GH, *et al*. Fast free-form deformable registration via calculus of variations. *Phys Med Biol* 2004;49:3067–3087.
19. Fletcher R, Reeves CM. Function minimization by conjugate gradients. *Comput J* 1964;7:149–154.
20. Yan H, Ren L, Godfrey DJ, *et al*. Accelerating reconstruction of reference digital tomosynthesis using graphics hardware. *Med Phys* 2007;34:3768–3776.